Carbon 169 (2020) 9–16

Contents lists available at ScienceDirect

Carbon

journal homepage: www.elsevier.com/locate/carbon

Perspectives

Inverse design of two-dimensional graphene/h-BN hybrids by a regressional and conditional GAN

Yuan Dong [a, 1], Dawei Li [a, 1], Chi Zhang [a], Chuhan Wu [b], Hong Wang [a], Ming Xin [a], Jianlin Cheng [b], Jian Lin [a, b, c, *]

[a] Department of Mechanical and Aerospace Engineering, USA
[b] Department of Electrical Engineering and Computer Science, USA
[c] Department of Physics and Astronomy, University of Missouri, Columbia, MO, 65211, USA

ARTICLE INFO

Article history:
Received 10 April 2020
Received in revised form
27 May 2020
Accepted 7 July 2020
Available online 22 July 2020

ABSTRACT

Design of materials with desired properties is currently laborious and heavily relies on intuition of researchers through a trial-and-error process. To tackle this challenge, we propose a novel regressional and conditional generative adversarial network (RCGAN) for inverse design of representative two-dimensional materials, the graphene and boron-nitride (BN) hybrids. RCGAN incorporates a supervised regressor network, thus overcoming the common technical barrier in the traditional unsupervised GANs, which cannot generate data when fed with continuous and quantitative labels. RCGAN can autonomously generate graphene/BN hybrids given any target bandgap values. These structures are distinguished from the ones used for training and exhibit high diversity for a given bandgap. Moreover, they exhibit high fidelity, yielding bandgaps within ~10% MAE_F of the desired bandgaps as validated by density functional theory (DFT) calculations. Analysis by the principle component analysis (PCA) and modified locally linear embedding (MLLE) reveals that the generator has successfully generated structures following the statistical distribution of the real structures. It implies the possibility of the RCGAN in recognizing physical rules hidden in the high-dimensional data. The novel strategy for designing regressional GAN architecture together with the successful application to inverse design of materials would inspire further exploration in research fields beyond materials.

1. Introduction

One of core objectives in material research is to correlate material structures and properties with a goal of designing novel materials. However, the searching spaces due to combination of the constituent elements and their structural configurations in the materials are massive, leading to an overwhelming number of potential candidates [1]. Although high-throughput computations [2], especially those based on the density functional theory (DFT), have enabled calculation of the structures and properties for various types of materials [3–6], the design principle is still limited by the search strategy, which heavily relies intuitions of the material scientists to explore the chemical space in a fixed library. In addition, the computational cost exponentially increases with the size of the systems. As a majority of functional materials possess the properties that cannot be simply determined by a few atoms, to accurately predict their properties by the physics-informed models a vast number of atoms and their possible spatial configurations should be considered in the calculations, which would make the calculations either impossible or not cost effective. *In silico* material design methods show a mechanism that may potentially solve this challenge. Some of them evolved from a Monte Carlo method [7] to the genetic search and cluster expansion approaches [8]. Although these approaches have made much progress in designing novel materials, the accuracy may decrease as the complexity of the systems increases. The efficacy is usually low due to the modality of generating one candidate after many evolution steps, thus they are not optimal for fast on-demand structural generation.

Therefore, development of surrogate models, such as machine learning models, has emerged in the era of big material data for mining established databases [9], previous literature [10], and

* Corresponding author.Department of Physics and Astronomy, University of Missouri, Columbia, MO, 65211, USA.
E-mail address: LinJian@missouri.edu (J. Lin).
[1] Authors contributed equally to this work.

https://doi.org/10.1016/j.carbon.2020.07.013
0008-6223/

experiments [11,12]. They can be also combined with the high-throughput computations for empowering the *in silico* design of materials with a much faster speed [1]. These synergetic strategies are expected to suitably tackle complex material challenges arising from the massive combinational chemical spaces or involving nonlinear processes, thereby being widely applied to develop functional materials such as inorganics [13,14], organic molecules [15], synthetic polymers [16], natural products [17], and metal-organic nanocapsules [18]. Feeding the deep neural networks with the computational data is particularly promising for handling and accelerating material discovery [19–21]. For instance, we recently developed convolutional neural network (CNNs) to accurately predict bandgaps of configurationally hybridized graphene and boron nitride (BN) with arbitrary BN dopant topographies [22]. Significance of the work was that it solved a challenge of predicting the bandgaps of the hybridized structures with a vast number of structural possibilities. Because the bandgaps can continuously evolve as change of the topographical configurations of C, B, N atoms in the structures, while the number of possibilities far exceeds what can be thoroughly computed due to the high computational cost from the DFT.

Nevertheless, this work as well as most of other related works were based on a forward design principle, in which target structures are hypothesized, evaluated against the target properties, and then iteratively refined based upon the results of repeated evaluations. As this iterative process tries to search for the optimum structures among the high multivariate and multidimensional parameters, it is hard to reason that the resulting ones meet such a goal. In contrast, an inverse design process starts from explicit calculation of the target performance metrics, thus realization of the target structures is much more efficient with higher fidelity [23]. Recently developed generative models, such as variational autoencoders (VAEs) and generative adversarial networks (GANs), have shown great potentials in automating this inverse design process [24]. For instance, a VAE was developed to generate molecules [25]. A critical novelty of this work is that the multilayer perceptron was connected with the latent vectors that represent the molecules for chemical property prediction. Although this reported VAE allows for search of new molecules with certain properties, the network still lacks a mechanism that can autonomously generate structures with given properties, which can be continuously and numerically labeled.

GANs possess some characteristics that may have superior advantages over the VAEs. They allow for interpolation using the input matrices provided to the generator. For instance, a GAN was introduced for the inverse design of metasurfaces with desired optical properties [26]. The discriminator and generator were simultaneously trained to output similar structures as the ones shown in specific training classes with the given optical spectra. The inverse design upon the desired spectra was attempted, but a large deviation between the desired spectra and obtained ones was observed. In a very recent study Gupta and Zou used Wasserstein GAN (WGAN) to generate DNA sequences with certain helix structures to realize target antimicrobial properties [27]. A function analyzer (deep recurrent neural network) was adopted to score the antimicrobial properties of the genes streamed from the generator. To score the properties of the helix structures, a black-box PSIPRED analyzer was used. Those genes with higher scores rated by the analyzer were fed to train the discriminator. Then the WGAN was updated for the next training epoch. This architecture was named a feedback GAN. Having the same limitation as shown in inverse design of metasurfaces [26], the feedback GAN cannot generate structures with given quantitative and continuous labels. Because these genes are classified into antimicrobial (yes or no) or helix (yes or no) groups. The generator can only obtain new structures that are similar to those in the specific classes.

Despite these seminal works, a GAN that enables inverse design of materials with explicitly given properties (represented by continuous labels) in an autonomous manner has been largely underexplored. The biggest challenge is that the GAN should meet both requirements: 1) it generates distinguished structures from the real structures used for training; 2) it should be able to accurately perform a generation task based on input quantitative labels. To achieve this, a regressional and conditional network would be needed. Ordinary GAN architectures including conditional GANs [28–30] have limitations in generating data conditioned on continuous and quantitative labels. Although some regressional GANs achieved initial success [31], the discriminator is not applied to tell the authenticity of data. To achieve that, extra ad-hoc parameter tuning is required. Thus, full autonomy of generating data in a regressional and conditional manner with high fidelity has yet been achieved.

To overcome the limitations shown in the previously developed GANs, we propose a novel GAN architecture that can perform both regressional and conditional tasks so that it can generate materials with target properties. We name it as regressional and conditional GAN (RCGAN). The key novelty of this RCGAN architecture is that it includes an extra regressional convolutional neural network (named as the regressor). The regressor outputs predicted bandgaps as well as vectors of the latent features from real and generated material structures (Fig. 1). These vectors are output from the second last layer of the regressor. Instead of directly using the generated structures and their bandgaps as the input to train the discriminator, the two sets of the latent features from the real and generated structures are concatenated with their corresponding bandgaps. They form two groups of vectors as the input to train the discriminator. This novel strategy enables better utilization of the automatic authentication from the discriminator. Thus, not only the generation function of the GAN is preserved, but also the generated structures can be associated with the target properties represented by the continuous and quantitative labels, leading to its successful application for the inverse materials design.

To demonstrate this capability, we present a case study by using two-dimensional graphene alloyed with the h-BN in arbitrary topographies. It was pointed out that in alloys the atomic configurations could strongly affect their properties, while enormous possible configurations make it impractical to exhaust even part of the configurations [32]. Our past study shows that these 2D hybrid structures have continuous and quantitative bandgaps which are not only determined by the concentration of BN pairs but also by the BN topographies [22]. The trained RCGAN can well reflect this structure-property relationship by showing generation of multiple yet distinguished graphene/BN structures upon given bandgap values. The bandgaps validated by the DFT are within ~10% MAE_F of the desired ones for various sizes of supercell systems. Further analysis by the PCA and MLLE methods reveals the working mechanism of the RCGAN. We envision that the inverse design of the materials with target properties in an autonomous manner, which is enabled by the demonstrated RCGAN, would push a step forward the self-driven material discovery [33]. Moreover, it would help scientists to discover new physical and chemical rules hidden in the high-dimensional data. Finally, with the function of generating data conditioned on continuous and quantitative labels, the RCGAN can be applied to data augmentation, imputation and etc.

2. Design and training of regressional and conditional GAN

2.1. Background

The original architecture of GAN proposed by Goodfellow et al.

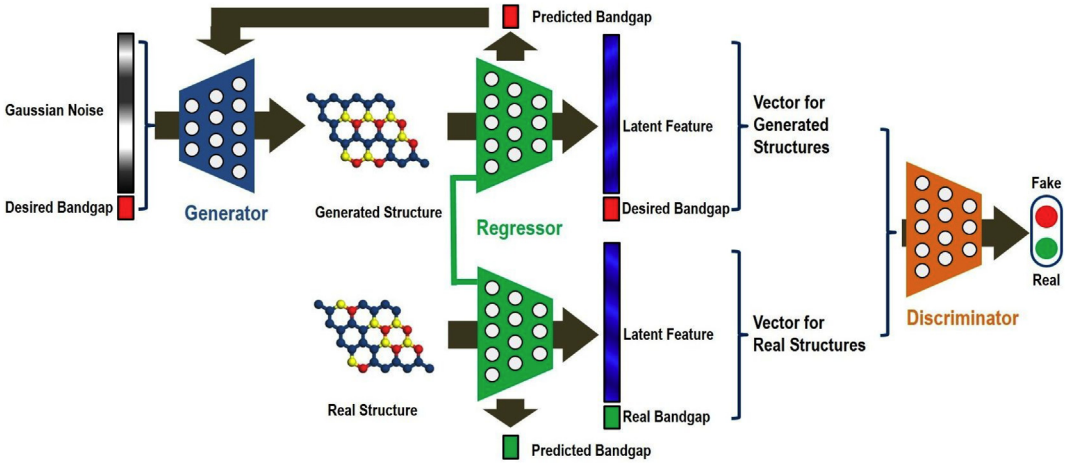

Fig. 1. Architecture of a proposed regressional and conditional GAN (RCGAN) for inverse structural design of 2D graphene/BN hybrids. (A colour version of this figure can be viewed online.)

consists of two competing networks, generator and discriminator [34]. The generator is able to generate data from a given random noise (Z). The data is then examined by the discriminator to see if it is synthesized (fake) or sampled from the training dataset (real). After the network is trained, a balance between the generator and discriminator is reached, and the generated data is so real that the discriminator cannot distinguish whether the data is generated from the generator or sampled from the training dataset. The original GAN is unsupervised. To enable on-demand data generation, the labeled information was added as the input condition to the networks to develop the conditional GAN (CGAN) [28]. Although CGAN generates data upon the input labels, the function is limited to image generation. Moreover, it only suits the labels that are discrete and represented by qualitative matrices. The later developed auxiliary classifier GAN (ACGAN) does not append the labels directly to the data that is fed to the discriminator [30]. Instead, the discrete and qualitative labels are adopted as a part of the objective function for training the ACGAN. In this case, the discriminator is still designed as a classifier. Thus, the ACGAN is only suited for problems that can be only represented by the discrete and qualitative labels.

A method of discretizing continuous labels according to its magnitude and then grouping them into multiple classes was previously adopted in our practice when we tested the ACGAN for generating graphene/BN structures with given bandgaps. But the generated structures have bandgaps that are far from the desired ones. It may be because binning labels in the same classes without knowing if the material structures share similar characteristics would violate the physical laws. A very recent semi-supervised reg-GAN was developed for generating images from the quantitative labels [31]. However, the reg-GAN discriminates the fake images from the real images by predicting the label first, then compares difference between the predicted label and the desired label. However, to do that, a preset ad-hoc range of the number is needed, which requires human intervention. Moreover, it deprives the function of automatic authentication from the discriminator. In summary, the past demonstrated GANs are notorious in network training, and face many problems like model divergence, mode collapse and overfitting of the generator. Mode collapse is a failure phenomenon that the generator finds such a way to generate a specific pattern (e.g. a graphene/BN structure in our case) that it can pass the examination of the discriminator, which makes the generation have no diversity or even meaningless [35]. Thus, they cannot meet the requirements for generating data in a regressional and conditional manner.

2.2. Architectures of regressor, generator, and discriminator

Herein, a RCGAN which generates the materials (e.g. graphene/BN hybrids) upon continuous and quantitative labels (e.g. bandgaps) was proposed (Fig. 1). In the RCGAN, the generator is a 9-layer CNN (Fig. S1). Batch normalization and leaky rectified linear unit (RELU) activation were applied after each deconvolution step to increase the network stability and accelerate the training process [36,37]. Deconvolution is a process that reverses the steps performed by a normal convolution. It was used to up-sample the matrices to satisfy the desired shape of the output matrices. The generator synthesizes the graphene/BN structures from Gaussian noise (Z, a 128 $\times$ 1 vector) and appended desired bandgaps (Y). As shown in Fig. S2, the regressor was modified from Google Inception V2 [38]. It was trained by using the dataset from the real graphene/BN structures. After trained, the regressor achieved a high prediction accuracy of >98% when validated by the test dataset by following the procedure shown in our past work [22]. A simple ANN network was recently proposed to predict energy gaps of graphene/h-BN [39]. This ANN network can be potentially used as the regressor of RCGAN to generate new configurations. The generated structures and sampled structures used for training were then fed into the regressor to achieve two goals. The first one is to accurately predict the bandgaps of given structures. The second one is to output the latent features for both generated and sampled structures. The latent features were then concatenated with their corresponding bandgaps to form two groups of vectors, which served as the input data for training the discriminator. The discriminator is a simple network that contains two fully connected layer intermediated by a dropout layer to prevent overfitting (Fig. S3). It has two main functions. The first one is to maintain the function of automatic authentication, while the second one is to determine if a generated structure corresponds to a desired bandgap. Detailed description on these three networks as well as creation of training data is illustrated in Supplementary Note 1.

2.3. Loss functions of regressor, generator, and discriminator

The loss function of the regressor is defined as the L_2 loss which indicates the difference between the predicted bandgaps from the regressor and desired bandgaps.

$$Loss_R = L_2[Y, R(X)] \quad (1)$$

The L_2 loss function is defined as

$$L_2[X,Y]=\sum_i\left(x_i-y_i\right)^2 \tag{2}$$

The loss function for the generator includes two terms. The first one is the same as the least square GAN(LSGAN) [40], while the second one is regularized from the regressor. The combined loss function is shown in the following equation.

$$Loss_G=\frac{1}{2}E_{z\sim P_z(z)}[D(\pi(G(z,Y)),Y)-1]^2+\lambda L_2(Y,R(G(z,Y))) \tag{3}$$

In Eq. (3), E is the expectation function. The subscript of $z \sim P_z(z)$ indicates that a graphene/BN structure is synthesized by the generator. $\pi(\cdot)$ is the latent vector extracted from the second last layer of the regressor when fed with graphene/BN structures. X and Y are the real structures and their bandgaps used for training, respectively. z is the random noise vector. D is the discrimination function. When feeding the regressor with the generated structures, the L_2 loss is calculated, and then used as the regularization term in the loss function of the generator. The regularization term is reweighted using a weighting parameter λ and added to the loss function of the generator as shown in Eq. (3). λ was chosen as 25 in this work to optimize the decrease of losses and improve generation performance. The first component of Eq. (3) is critical to bind the generator with the discriminator, which ensures simultaneous training of both networks. If only the second component of the loss function was used for the generator, the training was not successful because the loss of G and D did not descend but fluctuate at a relatively high level.

The loss function of discriminator is the same to the one used for LSGAN as shown in the following equation [40].

$$Loss_D=\frac{1}{2}E_{X\sim P_{data}(X)}[D(\pi(X),Y)-1]^2 +\frac{1}{2}E_{z\sim P_z(z)}[D(\pi(G(z,Y)),Y)]^2 \tag{4}$$

The subscript of $X \sim p_{data}(X)$ indicates that the structure was sampled from the real graphene/BN structures used for training.

3. Results and discussion

We trained the RCGAN with datasets created by DFT calculations which were previously used to study the properties of two-dimensional materials [22,41,42]. The details of DFT calculation is presented in the Supporting Information. Representative 4 × 4, 5 × 5, and 6 × 6 supercells of the graphene/BN structures and their corresponding material descriptors are shown in Fig. S4. These training datasets include 15,870 structures for the 4 × 4 systems, 80,647 structures for the 5 × 5 systems, and 85,808 structures for the 6 × 6 systems. They represent 24.2%, 0.24% and 0.0001% of all possible structures based on these three systems, respectively. Note that there could be many material structures in the training dataset having the translational or rotational equivalence. However, these equivalent materials are unique input to the deep learning models. It is also a data augmentation method to enlarge the training dataset. We traced the losses of the generator, regressor, and discriminator for the 4 × 4, 5 × 5 and 6 × 6 systems during the training processes and found that they gradually converged as the loss of the regressor was decreased. After 200 epochs of training, the loss of the regressor reached a steady-state plateau (Fig. S5). The magnitude of the loss reaches as low as 10^{-3}, indicating that the predicted bandgaps are quite close to the real bandgaps. The losses of the generator and discriminator also converged to stabilized values, indicating that balance of the two networks has been reached.

Performance of the RCGAN was evaluated by studying diversity and accuracy of the generated structures. Some examples of the generated structures with desired bandgaps are shown in Fig. 2. The generator outputs some structures which are equivalent to the real structures shown in the training datasets. But this situation only occupies ~12% of all generated structures for 4 × 4 systems, ~0.5% for 5 × 5 systems and zero for 6 × 6 systems. This result indicates that the RCGAN has been successfully trained without showing common problems such as the mode collapse happening during the GAN training. Take the generated 4 × 4 graphene/BN structures as an example (Fig. 2a–c). They are distinguished from the real structures in the training datasets. These generated structures have bandgaps that are very close to the desired ones as validated by DFT calculations. Moreover, they are quite diverse. Fig. 2d shows that the BN concentrations in the generated graphene/BN structures corresponding to a desired bandgap are widely distributed. For instance, the BN concentration varies from 25% to 62.5% for a desired bandgap of 1.1 eV, and it varies from 50% to 75% for a desired bandgap of 1.8 eV. It also confirms that the graphene/BN structures with the same BN concentration but different dopant topographies can have varied bandgaps. For example, the graphene/BN structures with 50% BN have the bandgaps ranging from 0.9 eV to 1.8 eV. This reflects the challenge in inverse design of the graphene/BN structures by the traditional methods due to a large variation in the chemical spaces and properties. It is possible that these generated materials may not be stable or realistic. Evaluation of stability could be done by calculating the energy above the convex hull, phonon spectrum, formation energy, and elastic modulus [41]. We expect that additional validation calculation from these perspectives could further confirm the stability of configurations exported from RCGAN. Furthermore, if the formation energy was also calculated for all configurations in the training dataset, we can use the Regressor in RCGAN to learn and predict the formation energy of newly designed configurations conveniently. This network can be appended to the current RCGAN to filter out the unstable configurations. We will explore this possibility in a future work.

Performance of the RCGAN in generating graphene/BN structures with larger supercell systems, e.g. 5 × 5 and 6 × 6 supercells, was also examined. Fig. 2e–g and Fig. S6 show examples of the generated 5 × 5 systems whose bandgaps were proved quite close to the desired ones. Fig. 2h shows a large range of BN concentrations in the generated graphene/BN structures, indicating the structural diversity. This performance is well maintained as the size of the supercell systems further increases to 6 × 6 (Fig. 2i-l). These results suggest that the RCGAN successfully captured the hidden information, such as the concentration and topographic distribution of the BN pairs in the real structures. We also successfully circumvented the common issues such as the mode collapse that often occurs during the GAN training process. It could be attributed to the tactic of using the latent features of the graphene/BN structures derived from the regressor, rather than simply using the structures as the input to train the discriminator.

Performance of the RCGAN was also analyzed by evaluating the bandgaps of the generated structures with desired ones (Fig. 3). Fig. 3a shows that the bandgaps (E_{GB}) of the generated 4 × 4 structures have good linear relationship with the desired bandgaps (E_{DB}). The correlation factor, R^2, is 0.87. We also studied the relative error between E_{GB} and E_{DB}, calculated as $|E_{DB}-E_{GB}|/E_{DB}$. Fig. 3b shows that 64% of the generated 4 × 4 structures have bandgaps within a 10% relative error. This number increases to >85% if the bandgaps are within a 20% relative error. The fractional mean absolute error (MAE_F) (Supplementary Note 2) between E_{GB} and E_{DB} is as low as 9.45% for the 4 × 4 systems. Fig. 3c shows that R^2 reaches

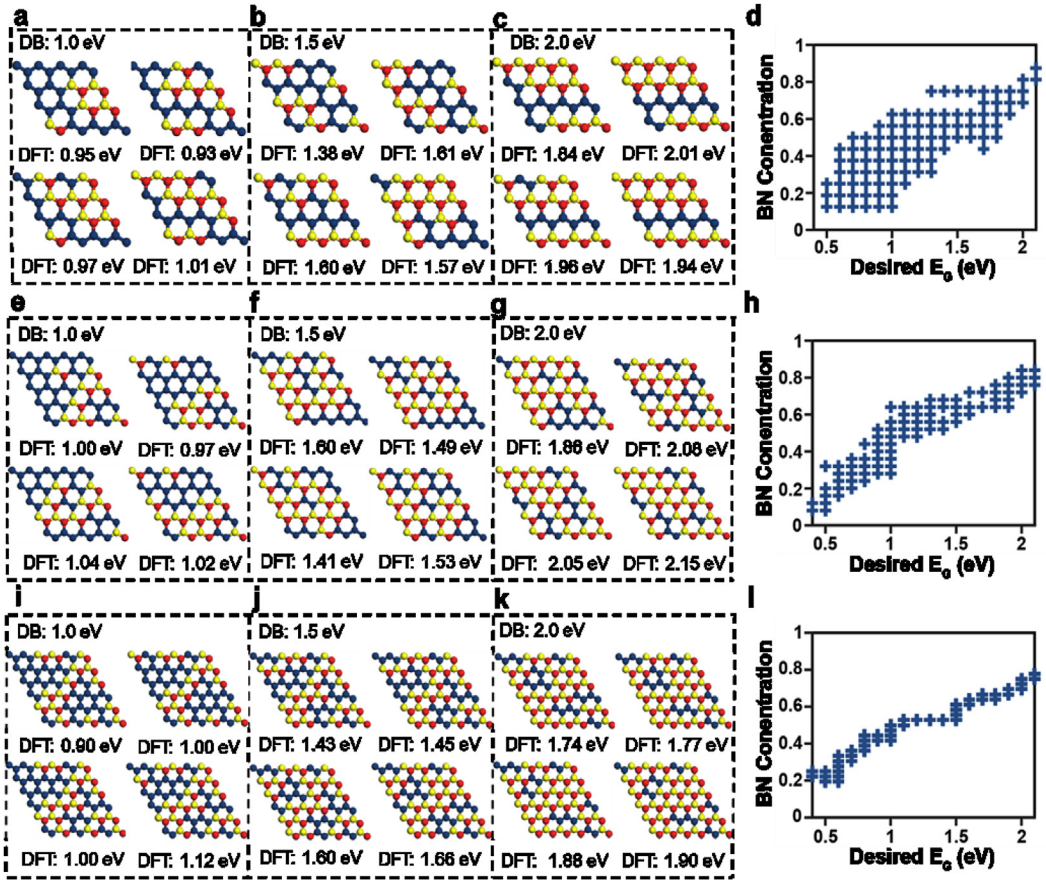

Fig. 2. Typical generated structures with desired bandgaps of (a) 1.0 eV, (b) 1.5 eV, and (c) 2.0 eV for 4 × 4 supercell systems. (d) BN concentration of generated structures vs. desired bandgaps for 4 × 4 supercell systems. Typical generated structures with desired bandgaps of (e) 1.0 eV, (f) 1.5 eV, (g) 2.0 eV for 5 × 5 supercell systems. (h) BN concentration of generated structures vs. desired bandgaps for 5 × 5 supercell systems. Typical generated structures with desired bandgaps of (i) 1.0 eV, (j) 1.5 eV, (k) 2.0 eV for 6 × 6 supercell systems. (l) BN concentration of generated structures vs. desired bandgaps for 6 × 6 supercell systems. The C, B, N atoms are colored with blue, red and yellow, respectively. (A colour version of this figure can be viewed online.)

0.90 for the 5 × 5 systems. This value is as good as the one predicted by the CNNs in a forward design task [22]. Fig. 3d shows that ~50% of the generated 5 × 5 structures whose bandgaps fall within a relative error of 10%, while <20% of the structures have a relative error of 20% or more. The MAE_F of the 5 × 5 systems is 10.78%. Accuracy of the RCGAN is well maintained as the size of the supercell increases to 6 × 6. Fig. 3e shows that R^2 of all generated 6 × 6 structures reaches 0.97. About 58.7% of them have bandgaps within a relative error of 10%. < 15% of them have a relative error of 20% or more. MAE_F of 6 × 6 systems is 10.36%, smaller than the one from 5 × 5 systems. Even though the sampling ratio of 6 × 6 systems (1e-4%) is much smaller than that of 5 × 5 systems (0.24%), the well maintained performance indicates the robustness of the RCGAN. If characterized by MAE_F, the developed RCGAN shows the generation accuracy exceeding recent works of using GAN for inverse material design [26,27]. We anticipate that the accuracy could be further improved by adding more training data and further optimizing the networks.

Successful generation of the graphene/BN structures with the desired bandgaps by the proposed RCGAN motivates us to hypothesize that the latent features encoded by the regressor help to associate the generated structures with their bandgaps. To test this hypothesis, a key idea is to validate whether the latent features of the structures synthesized from the generator has successfully followed the statistical distribution of the real structures used for training. Thus, we performed dimension reduction analysis on both of them by the principal component analysis (PCA) [43] and modified locally linear embedding (MLLE) [44] (Supplementary Note 3). Fig. 4a shows mapping of the first and second components of PCA (PCA_X and PCA_Y) of the latent features from 1000 4 × 4 real structures and 1000 4 × 4 generated structures. They are highly overlapped, suggesting that the RCGAN has successfully learned the distribution of the latent vectors from the real structures for generating new structures. Fig. 4b shows that the PCA_X has a good linear relationship to the bandgaps (labels). This linear correlation between PCA_X and bandgaps is impressive. In a previous work, it is found that the PCA_X, i.e. the first or the major component in the latent feature, could capture a significant part of the variance for predicting the flexoelectricity of materials [45]. Compared to this work, we hypothesize that PCA_X shown in Fig. 4b is strongly correlated with the BN concentration. It indicates that the generator may catch the physical law that the bandgap increases with the increase of the BN concentration, which agrees well with the results suggested from the real structures used for training (Fig. 4c). The curve of the bandgap vs. PCA_Y shows that the generated structures can be grouped into two regions (Fig. 4d). The structures with high bandgaps (>~1.0 eV) are in one region, while the ones with lower bandgaps (<~1.0 eV) are in the other.

In addition to the PCA, we also performed the MLLE analysis. Two sets of data points from the real and generated structures form a well overlapped parabolic curve (Fig. 4e). It suggests that the MLLE can well capture the relationship between structural

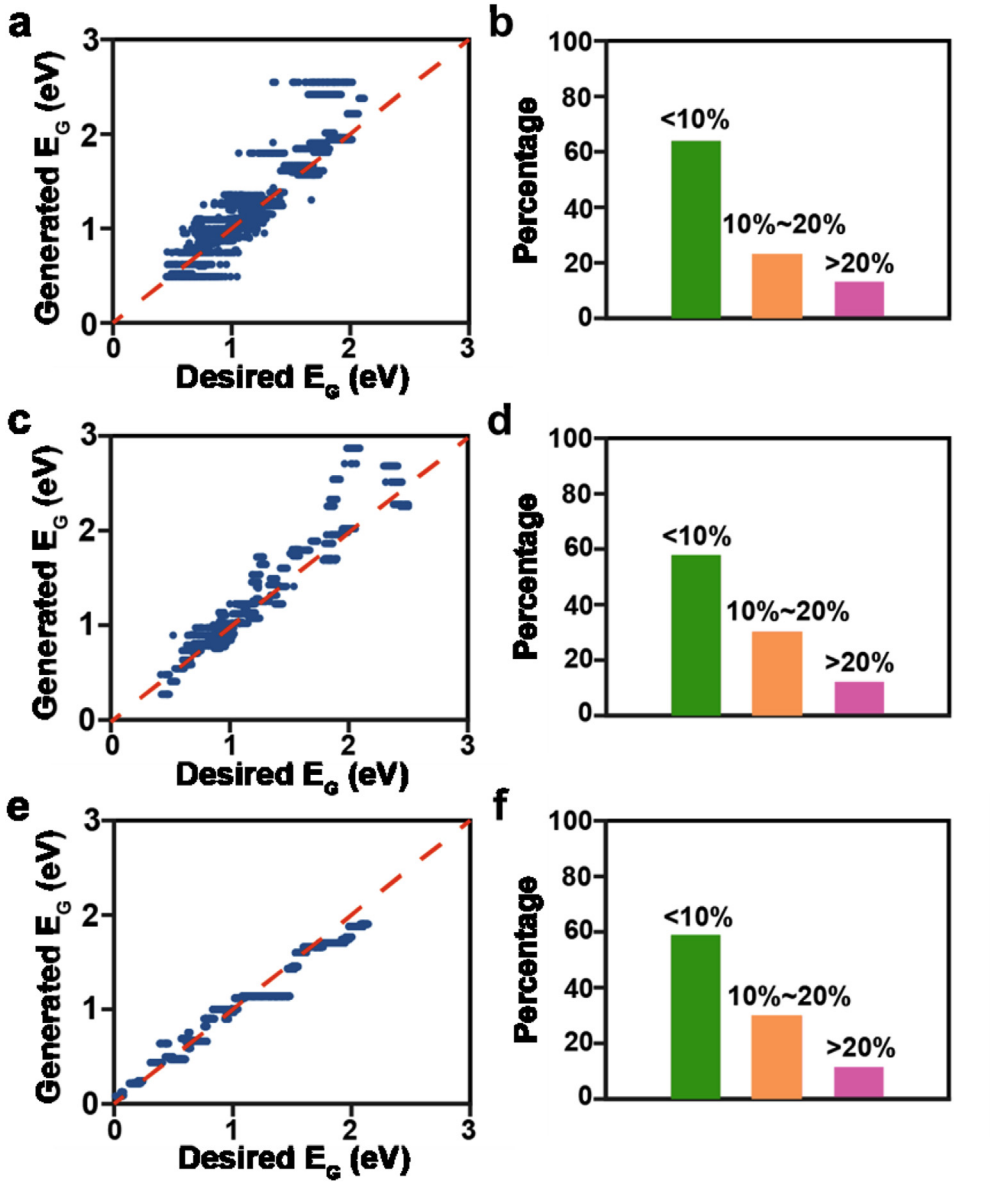

Fig. 3. (a) Bandgaps of generated structures validated by DFT vs. desired input bandgaps for 4 × 4 supercell systems, $R^2 = 0.87$. (b) Error distribution of bandgaps for generated 4 × 4 supercell systems, $MAE_F = 9.45\%$. (c) Bandgaps of generated structures validated by DFT vs. desired input bandgaps for 5 × 5 supercell systems, $R^2 = 0.90$. (d) Error distribution of bandgaps for generated 5 × 5 supercell systems, MAEF = 10.75%. (e) Bandgaps of generated structures validated by DFT vs. desired input bandgaps for 6 × 6 supercell systems, $R^2 = 0.97$. (f) Error distribution of bandgaps for generated for 6 × 6 supercell systems, MAEF = 10.36%. (A colour version of this figure can be viewed online.)

configurations and bandgaps. The mapped bandgaps of the generated structures vs. the first and second components of the MLLE results are shown in (Figs. S7a–b). They illustrate that these data points have similar trend as the ones shown in the PCA. It also indicates that the bandgaps monotonically increase as the $MLLE_x$ increases. Further analysis on the structural evolution along the path shown in the MLLE curve suggests that the location and concentration of BN pairs gradually change as the bandgap values increases (Fig. 4f). Their neighboring structures share similar BN topographies with limited discrepancy.

4. Conclusion

In this work, we proposed a novel RCGAN for inverse structural design of a representative 2D material given quantitative properties. Extraction and usage of the latent features encoded from the regressor as the input for training the discriminator was critical to successfully train the RCGAN. Not only can this architecture generate data autonomously, accurately and robustly, but also avoid problems during typical GAN training processes like overfitting and mode collapse. To the best of our knowledge, this is the first time of using this strategy for designing regressional and conditional GAN. The generated structures follow the statistic distribution of the real structures used for training as validated by the dimensional reduction analysis. Statistically, the bandgaps of the generated structures are very close to the desired bandgaps, exhibiting MAE_F of ~9.45%, 10.78%, and 10.36% for 4 × 4, 5 × 5, and 6 × 6 systems, respectively. This illustrative example shows the power of the proposed RCGAN in accurately designing materials with target properties in an autonomous manner. In particular, the graphene/BN structures generated by RCGAN correspond to bandgaps ranging from 0.5 eV to 2.0 eV, indicating that functional materials

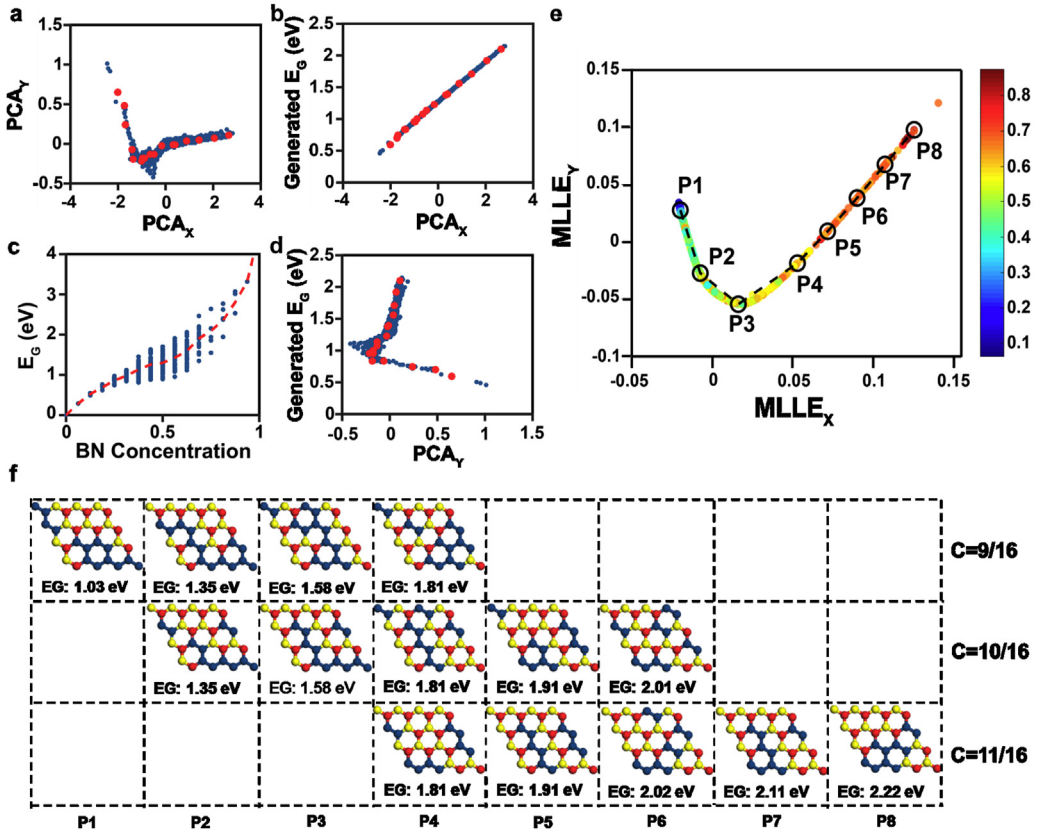

Fig. 4. PCA and MLLE analysis on the latent features of 4 × 4 supercell systems encoded by the regressor. **(a)** Mapping of PCA_X and PCA_Y components. Blue dots are the training data. Red dots are the generated data. **(b)** Relationship of bandgap of generated structures vs. PCA_x. **(c)** Bandgaps of real structures vs. BN concentrations. **(d)** Relationship of bandgap of generated structures vs. PCA_Y. **(e)** Mapping of $MLLE_X$ and $MLLE_Y$ from real and generated structures. The dots represent points in the datasets. Colors of the dots represent the BN concentration in graphene/BN structures. **(f)** Structural evolution along the points (P1−P8) marked in **(e)**. C indicates the BN concentration. (A colour version of this figure can be viewed online.)

with tunable properties can be obtained. This success would open new possibilities for the RCGAN to be applied to fields such as electronics, photovoltaic, and photocatalysis. It will offer a brand-new platform for highly automated on-demand material design that is enabled by big material data and artificial intelligence. Moreover, the proposed RCGAN can be used for data augmentation and imputation, thus broadening its impacts on other fields beyond materials.

Data availability

All data needed to evaluate the conclusions in the paper are present in the paper and/or the Supplementary Materials. Additional data related to this paper may be requested from the authors. Supplementary code is available at https://github.com/linresearchgroup/RCGAN_Graphene.

CRediT authorship contribution statement

Yuan Dong: Formal analysis, Writing - original draft. **Dawei Li:** Writing - original draft. **Chi Zhang:** Formal analysis. **Chuhan Wu:** Software. **Hong Wang:** Formal analysis. **Ming Xin:** Project administration. **Jianlin Cheng:** Supervision. **Jian Lin:** Project administration, Writing - original draft, Writing - original draft.

Declaration of competing interest

The authors declare that they have no known competing financial interests or personal relationships that could have appeared to influence the work reported in this paper.

Acknowledgement

J. L. and M.X. acknowledge financial support from US Department of Energy (Award number: DE-FE0031645). J. L. thanks National Science Foundation (Award number: 1825352 and 1933861). J. C. acknowledges National Science Foundation (Award numbers: DBI1759934 and IIS1763246). The DFT calculations were performed on the HPC resources at the University of Missouri Bioinformatics Consortium (UMBC), supported in part by NSF (award number: 1429294). Y.D. acknowledges the startup funding of Hangzhou Dianzi University.

Appendix A. Supplementary data

Supplementary data to this article can be found online at https://doi.org/10.1016/j.carbon.2020.07.013.

References

[1] K.T. Butler, D.W. Davies, H. Cartwright, O. Isayev, A. Walsh, Machine learning for molecular and materials science, Nature 559 (7715) (2018) 547.
[2] S. Curtarolo, G.L. Hart, M.B. Nardelli, N. Mingo, S. Sanvito, O. Levy, The high-throughput highway to computational materials design, Nat. Mater. 12 (3) (2013) 191.
[3] J. Hachmann, R. Olivares-Amaya, S. Atahan-Evrenk, C. Amador-Bedolla, R.S. Sánchez-Carrera, A. Gold-Parker, et al., The Harvard clean energy project: large-scale computational screening and design of organic photovoltaics on

the world community grid, J. Phys. Chem. Lett. 2 (17) (2011) 2241–2251.
[4] E.O. Pyzer-Knapp, C. Suh, R. Gómez-Bombarelli, J. Aguilera-Iparraguirre, A. Aspuru-Guzik, What is high-throughput virtual screening? A perspective from organic materials discovery, Annu. Rev. Mater. Res. 45 (2015) 195–216.
[5] R. Gómez-Bombarelli, J. Aguilera-Iparraguirre, T.D. Hirzel, D. Duvenaud, D. Maclaurin, M.A. Blood-Forsythe, et al., Design of efficient molecular organic light-emitting diodes by a high-throughput virtual screening and experimental approach, Nat. Mater. 15 (10) (2016) 1120–1127.
[6] J. Carrete, W. Li, N. Mingo, S. Wang, S. Curtarolo, Finding unprecedentedly low-thermal-conductivity half-Heusler semiconductors via high-throughput materials modeling, Phys. Rev. X 4 (1) (2014), 011019.
[7] A. Franceschetti, A. Zunger, The inverse band-structure problem of finding an atomic configuration with given electronic properties, Nature 402 (6757) (1999) 60–63.
[8] A. Zunger, Inverse design in search of materials with target functionalities, Nature Reviews Chemistry 2 (4) (2018) 1–16.
[9] C.E. Calderon, J.J. Plata, C. Toher, C. Oses, O. Levy, M. Fornari, et al., The AFLOW standard for high-throughput materials science calculations, Comput. Mater. Sci. 108 (2015) 233–238.
[10] V. Tshitoyan, J. Dagdelen, L. Weston, A. Dunn, Z.Q. Rong, O. Kononova, et al., Unsupervised word embeddings capture latent knowledge from materials science literature, Nature 571 (7763) (2019) 95–98.
[11] P. Raccuglia, K.C. Elbert, P.D.F. Adler, C. Falk, M.B. Wenny, A. Mollo, et al., Machine-learning-assisted materials discovery using failed experiments, Nature 533 (7601) (2016) 73–76.
[12] J.-P. Correa-Baena, K. Hippalgaonkar, J. van Duren, S. Jaffer, V.R. Chandrasekhar, V. Stevanovic, et al., Accelerating materials development via automation, machine learning, and high-performance computing, Joule 2 (8) (2018) 1410–1420.
[13] E. Kim, K. Huang, S. Jegelka, E. Olivetti, Virtual screening of inorganic materials synthesis parameters with deep learning, npj Computational Materials 3 (1) (2017) 53.
[14] Q. Li, C. Nelson, S.-L. Hsu, A. Damodaran, L.-L. Li, A. Yadav, et al., Quantification of flexoelectricity in PbTiO 3/SrTiO 3 superlattice polar vortices using machine learning and phase-field modeling, Nat. Commun. 8 (1) (2017) 1468.
[15] D.C. Elton, Z. Boukouvalas, M.D. Fuge, P.W. Chung, Deep learning for molecular design—a review of the state of the art, Molecular Systems Design & Engineering 4 (2019) 828–849.
[16] A. Mannodi-Kanakkithodi, A. Chandrasekaran, C. Kim, T.D. Huan, G. Pilania, V. Botu, et al., Scoping the polymer genome: a roadmap for rational polymer dielectrics design and beyond, Mater. Today 21 (7) (2018) 785–796.
[17] M.H. Medema, M.A. Fischbach, Computational approaches to natural product discovery, Nat. Chem. Biol. 11 (9) (2015) 639.
[18] Y. Xie, C. Zhang, X. Hu, C. Zhang, S.P. Kelley, J.L. Atwood, et al., Machine learning assisted synthesis of metal-organic nanocapsules, J. Am. Chem. Soc. 142 (3) (2020) 1475–1481.
[19] J.J. de Pablo, N.E. Jackson, M.A. Webb, L.-Q. Chen, J.E. Moore, D. Morgan, et al., New frontiers for the materials genome initiative, npj Computational Materials 5 (1) (2019) 41.
[20] A. Jain, S.P. Ong, G. Hautier, W. Chen, W.D. Richards, S. Dacek, et al., Commentary: the Materials Project: a materials genome approach to accelerating materials innovation, Apl. Mater. 1 (1) (2013), 011002.
[21] H. Wang, Y. Xie, D. Li, H. Deng, Y. Zhao, M. Xin, et al., Rapid identification of X-ray diffraction patterns based on very limited data by interpretable convolutional neural networks, J. Chem. Inf. Model. 60 (4) (2020) 2004–2011.
[22] Y. Dong, C. Wu, C. Zhang, Y. Liu, J. Cheng, J. Lin, Bandgap prediction by deep learning in configurationally hybridized graphene and boron nitride, npj Computational Materials 5 (1) (2019) 26.
[23] L. Hou, R.J. Jiao, Data-informed inverse design by product usage information: a review, framework and outlook, J. Intell. Manuf. (2019) 1–24.
[24] B. Sanchez-Lengeling, A. Aspuru-Guzik, Inverse molecular design using machine learning: generative models for matter engineering, Science 361 (6400) (2018) 360–365.
[25] R. Gómez-Bombarelli, J.N. Wei, D. Duvenaud, J.M. Hernández-Lobato, B. Sánchez-Lengeling, D. Sheberla, et al., Automatic chemical design using a data-driven continuous representation of molecules, ACS Cent. Sci. 4 (2) (2018) 268–276.
[26] Z. Liu, D. Zhu, S.P. Rodrigues, K.-T. Lee, W. Cai, Generative model for the inverse design of metasurfaces, Nano Lett. 18 (10) (2018) 6570–6576.
[27] A. Gupta, J. Zou, Feedback GAN for DNA optimizes protein functions, Nature Machine Intelligence 1 (2) (2019) 105–111.
[28] M. Mirza, S. Osindero, Conditional Generative Adversarial Nets, 2014 arXiv preprint arXiv:14111784.
[29] P. Isola, J.-Y. Zhu, T. Zhou, A.A. Efros, Image-to-image translation with conditional adversarial networks, Proceedings of the IEEE Conference on Computer Vision and Pattern Recognition (2017) 1125–1134.
[30] A. Odena, C. Olah, J. Shlens, Conditional image synthesis with auxiliary classifier gans, Proceedings of the 34th International Conference on Machine Learning 70 (2017) 2642–2651.
[31] M. Rezagholiradeh, M.A. Haidar, Reg-Gan: semi-supervised learning based on generative adversarial networks for regression, in: IEEE International Conference on Acoustics, Speech and Signal Processing, 2018, pp. 2806–2810.
[32] A. Zunger, S.H. Wei, L.G. Ferreira, J.E. Bernard, Special quasirandom structures, Phys. Rev. Lett. 65 (3) (1990) 353–356.
[33] F. Häse, L.M. Roch, A. Aspuru-Guzik, Next-generation experimentation with self-driving laboratories, Trends in Chemistry 1 (3) (2019) 282–291.
[34] I. Goodfellow, J. Pouget-Abadie, M. Mirza, B. Xu, D. Warde-Farley, S. Ozair, et al., Generative adversarial nets, Adv. Neural Inf. Process. Syst. (2014) 2672–2680.
[35] M. Arjovsky, S. Chintala, L. Bottou, Wasserstein gan, 2017 arXiv preprint arXiv: 170107875.
[36] S. Ioffe, C. Szegedy, Batch Normalization: Accelerating Deep Network Training by Reducing Internal Covariate Shift, 2015 arXiv preprint arXiv:150203167.
[37] A.L. Maas, A.Y. Hannun, A.Y. Ng, Rectifier nonlinearities improve neural network acoustic models, in: Proceedings of the 30 Th International Conference on Machine Learning, 2013, p. 3. Atlanta, Georgia, USA.
[38] C. Szegedy, W. Liu, Y. Jia, P. Sermanet, S. Reed, D. Anguelov, et al., Going deeper with convolutions, Proceedings of the IEEE conference on Computer Vision and Pattern Recognition (2015) 1–9.
[39] T.L. Mitran, G.A. Nemnes, Prediction of energy gaps in graphene-hexagonal boron nitride nanoflakes uing artificial neural networks, in: E. Levchenko, Y. Dappe, G. Ori (Eds.), Theory and Simulation in Physics for Materials Applications, Springer, Cambridge, 2020.
[40] X. Mao, Q. Li, H. Xie, R.Y. Lau, Z. Wang, S. Paul Smolley, Least squares generative adversarial networks, Proceedings of the IEEE International Conference on Computer Vision (2017) 2794–2802.
[41] Y. Dong, C. Zhang, M. Meng, M.M. Groves, J. Lin, Novel two-dimensional diamond like carbon nitrides with extraordinary elasticity and thermal conductivity, Carbon 138 (2018) 319–324.
[42] Y. Dong, M. Meng, M.M. Groves, C. Zhang, J. Lin, Thermal conductivities of two-dimensional graphitic carbon nitrides by molecule dynamics simulation, Int. J. Heat Mass Tran. 123 (2018) 738–746.
[43] J. Lever, M. Krzywinski, N. Altman, Principal component analysis, Nat. Methods 14 (2017) 641.
[44] Z. Zhang, J.M.L.L.E. Wang, Modified locally linear embedding using multiple weights, Adv. Neural Inf. Process. Syst. (2007) 1593–1600.
[45] Q. Li, C. Nelson, S.-L. Hsu, A.R. Damodaran, L.-L. Li, A. Yadav, et al., Quantification of flexoelectricity in PbTiO 3/SrTiO 3 superlattice polar vortices using machine learning and phase-field modeling, Nat. Commun. 8 (1) (2017) 1468.